Supplement to "Detailed source term estimation of the atmospheric release for the Fukushima Daiichi Nuclear Power Station accident by coupling simulations of atmospheric dispersion model using improved deposition scheme and oceanic dispersion model"

G. Katata[1], M. Chino[1], T. Kobayashi[1], H. Terada[1], M. Ota[1], H. Nagai[1], M. Kajino[2], R. Draxler[3], M. C. Hort[4], A. Malo[5], T. Torii[6] and Y. Sanada[7]

[1]{Japan Atomic Energy Agency (JAEA), Tokai, Naka, Ibaraki, 319-1195, Japan; now at Atmospheric Environmental Research, Institute of Meteorology and Climate Research, Karlsruhe Institute of Technology, Germany}
[2]{Meteorological Research Institute, Japan Meteorological Agency (JMA), Tsukuba, Ibaraki, 305-0052, Japan}
[3]{Air Resources Laboratory, National Oceanic and Atmospheric Administration (NOAA), University Research Court College Park, Maryland 20740, USA}
[4] {Met Office, Exeter, Devon EX1 3PB, United Kingdom}
[5] {Canadian Meteorological Centre (CMC), Dorval, Quebec, H9P 1J3, Canada}
[6]{JAEA, Chiyoda, Tokyo, 100-8577, Japan}
[7]{JAEA, Fukushima, Fukushima, 960-1296, Japan}
Correspondence to: G. Katata (katata.genki@jaea.go.jp)

Preliminary analysis of deposition process using modified WSPEEDI

Figure S5 shows the spatial maps of modeled cumulative dry and wet deposition for each radionuclide. Cumulative dry deposition of ^{131}I was large and in the order of gaseous I_2, particulate iodine, and gaseous CH_3I as indicated by the order of modeled deposition velocities (Fig. A1). Large dry deposition of gaseous I_2 over the ocean was caused by high release rates on the order of 10^{14} Bq h^{-1} and a large gas fraction up to 67% of ^{131}I from 22–24 March. These results indicate that both the gas and particle forms are important to predict the total dry deposition of ^{131}I in FNPS1 accident. In contrast, wet deposition of I_2 and CH_3I were significantly lower than that of particles due to the solubility of gas species as modeled in Eq. (A7) (Fig. S5b). This indicates that the gas species of ^{131}I did not contribute to the contamination of East Japan.

As shown in Fig. S5b, in the WSPEEDI simulation, a large part of regional-scale contamination was derived from in-cloud scavenging of particulate species; e.g., large deposition of ^{137}Cs in Fukushima, Gunma, and Tochigi Prefectures. This deposition was reproduced by using high values of scavenging coefficient (Λ) ranging from 10^{-4}–10^{-2} s^{-1} on 15 March (Fig. S6) and which shows a result similar to the WRF-CMAQ atmospheric dispersion simulation (Morino et al., 2013). However, there is an unresolved issue regarding precipitation rates versus scavenging efficiency as both models overestimated the observed precipitation amount over Tochigi and Gunma Prefectures (Fig. S1). This is also apparent in comparisons between the calculation results of NAME-MSM and NAME-MSM-RAP (next section). Such overestimation of precipitation was found at Yamagata Prefecture in the evening on 20 March (Fig. S1). Further work with improved precipitation fields for atmospheric dispersion simulations is clearly required to quantify the impact of in-cloud scavenging.

As described in Terada et al. (2012) and Kaneyasu et al. (2012), fog and drizzle were observed in the above region and Naka-Dori in the afternoon on 15 March. Figure S7a illustrates the distribution of calculated cumulative fogwater deposition of ^{137}Cs. In the WSPEEDI simulation, fogwater deposition does not make a large contribution to the total deposition (Fig. S7a) compared with wet deposition (Fig. S5b). However, the model clearly underestimated observed cloud liquid water content (CLW) derived from visibility data at Okunikko and Karuizawa in the afternoon on 15 March (Fig. S7a, Fig. S8), while modeled rainfall was overestimated (Fig. S1). Moreover, the microphysics and fogwater deposition schemes do not explicitly consider drizzle deposition, i.e., horizontal wind-driven precipitation of large droplets (typically 100–500 μm in diameter). Since the spatial pattern of calculated fog deposition was consistent with the large contamination areas in Tochigi and Gunma Prefectures (Fig. S7a), fog and drizzle may have contributed to the contamination in the area.

Figures S7b–f depict the spatial patterns of CCN activation fraction (f_{ccn}) and the accretion efficiency of cloud droplets by settling ice crystals (i.e., snow and graupel) (f_{ice}) averaged for the atmospheric layers where the calculated plume existed. On 15 and 20 March, although most of areas showed the complete activation of aerosols ($f_{ccn}\approx1$), aerosols were not completely activated on the windward side of the mountains in Gunma and Tochigi Prefectures. This is because the modeled vertical wind velocity was weak (<0.1 m s^{-1}) in orographic clouds. In contrast, when the plume from FNPS1 flowed toward the southwestern direction on 21 March, aerosols in the plume were completely activated over the flat terrain of the Kanto region (Fig. S7f). This indicates that predicting the activation fraction of aerosols

(i.e., aerosol size, hygroscopicity, and vertical wind velocity) is also important to the wet scavenging of radionuclides over the complex terrain.

On 15 and 20 March, ice crystals enhanced the wet scavenging up to 1.2 times the scavenging coefficient of rain droplets along the plume pathway (Figs. S7c and e) due to the high accretion rate of clouds by ice crystals compared with that by raindrops. This increase was mainly observed in the north part of Fukushima Prefecture and Tohoku region during the FNPS1 accident because the water content consisted of large amounts of ice crystals under low air temperature conditions.

The total regional scale deposition budget was calculated in the WSPEEDI simulation using the new source term (Table S2). Twenty eight percent of the total ^{137}Cs release deposited to the land over East Japan, while 6.6% deposited onto the ocean near the coast. Sixty seven percent of ^{137}Cs discharged from FNPS1 flowed out of the region, which was larger than estimated in prior studies using our previous source term (42% in Terada et al., 2012; 54% in Morino et al., 2013). The change is primarily because the release rates when the plume directly flowed toward the ocean significantly increased from our prior source term (Table 8).

As shown in Table S2, wet deposition mainly caused the contamination areas over the land and accounts for 20% to the total release amount. Dry deposition only accounted for 5% of total release amount onto the land around the plant (Fig. S5a), which was clearly larger than that of the prior study (Morino et al., 2013). This difference is considered to be due to increases in the source term and dry deposition velocity. Although only 1.5% of the release was removed by fogwater, this value may change if rainfall amount and drizzle and fog events in Tochigi and Gunma Prefectures are correctly reproduced by the model as discussed above.

For the ecological assessment of radionuclides, deposition amounts of ^{137}Cs to the forest areas in East Japan (Fig. 3) were calculated from the WSPEEDI simulation. A large part of ^{137}Cs discharged from the plant deposited to forest areas (18%), corresponding to 65% of total deposition over East Japan. The wet deposition was also dominant in forest representing 14% of the total release amount compared with 3.1% for dry and 0.8% for fogwater deposition.

Preliminary analysis of deposition patterns using WMO models

In this subsection, the impact of the wet scavenging schemes on the deposition patterns is discussed based on the comparisons between observations and calculations of three WMO models (MLDP0, HYSPLIT, and NAME). In Fig. 19, MLDP0 generally showed underestimation of measurements as indicated from the slope less than the unity. This model does not use the precipitation field directly as other atmospheric transport and dispersion models. Wet deposition is treated with a simple scheme and will occur when a particle is presumed to be in a cloud (in-cloud scavenging) and is modeled in terms of a wet scavenging rate. The tracer removal rate is proportional to the wet scavenging coefficient, the local cloud fraction (parameterized as a function of relative humidity), and the particle mass. Thus, low values of the wet scavenging coefficient on the order of 10^{-5} s^{-1} as in the original WSPEEDI-II (Fig. A2b) and/or the cloud fraction may contribute to the underestimation of ^{137}Cs deposition measurements. In contrast, HYSPLIT and NAME showed the larger slope value close to the unity as shown in Fig. 19 because the model applies the large value of scavenging coefficient generally on the order of 10^{-4}–10^{-3} s^{-1} and considers the enhancement of wet deposition due to in-cloud scavenging and orographical (seeder-feeder) effects under both rain and snow situations. This is similar to the value of scavenging coefficient in our modified scheme with

small cloud liquid water content (Fig. A2b), resulting in the good correlation to the calculation results in the WSPEEDI simulation (Fig. 16). Similar results were also obtained in the parametric study of Morino et al. (2013) by changing the scavenging coefficient in the CMAQ atmospheric dispersion model.

To evaluate the surface deposition patterns under different meteorological conditions, three meteorological data sets were utilized with the atmospheric dispersion model NAME (Jones et al., 2007) using the new source term: 1) the Meso-Scale Model (MSM) with 3-hour precipitation by the Japan Meteorological Agency (JMA), 2) the MSM wind fields but using the JMA radar/rain gauge-analyzed precipitation fields (MSM-RAP, 1-km resolution at 30-min intervals), and 3) European Centre for Medium-Range Weather Forecasts (ECMWF, 0.125° resolution at 3-hour intervals). Figure S9a compares the spatial distributions of cumulative deposition of ^{137}Cs calculated by NAME with the different meteorological input data. Although the highest dose rate zone lay northwest from FNPS1 in all the calculation results, several differences were found in the deposition patterns in East Japan when they were compared with observations from the airborne survey. For example, the observed high deposition region along the mountain areas in Tochigi and Gunma Prefectures was not reproduced in the calculations of NAME-MSM-RAP. This is because very little precipitation was detected by the radar/rain gauge observations when the plume passed over those regions during the afternoon on 15 March. This indicates that both NAME-MSM and NAME-ECMWF have a possibility to overestimate observed precipitation in this region. Furthermore, NAME-ECMWF calculations produced a large amount of surface deposition to the northwest near FNPS1 compared with NAME-MSM and NAME-MSM-RAP. This is caused by the overestimation of precipitation intensity near the plant calculated by ECMWF (not shown in the figure). As shown in scatter plots comparing observations with calculations (Fig. S9b), the prediction accuracy seems to be the best when the input data of MSM are used with the NAME model.

Table S1. Statistics of the air concentrations of ^{131}I and ^{137}Cs between observations at various monitoring sites [KEK, RIKEN, JCAC, and Tokyo Metropolitan Government (IRI)] and calculations using all combinations of original and modified WSPEEDI-II (referred as "Old model" and "New model", respectively) and Terada at al. (2012) and the new source terms (referred as "Terada" and "New", respectively). Six statistical parameters were selected to represent different evaluation metrics: the correlation coefficient (CC), the fractional bias (FB), the normalized mean square error (NMSE), and the percent within a factor of two, five, and ten (FA2, FA5, FA10). The data were compared with calculations of WSPEEDI-II over domain 2. Note that only the data > 0.01 Bq m^{-3} were analyzed to compare when the plume passed through. Measured and calculated daily mean values at IRI were compared to reduce the error due to the discrepancy in the plume movement between the measurement and calculation.

Source term & model	CC	FB	NMSE	FA2	FA5	FA10
^{137}Cs air concentration from 15 March to 1 April 2011						
Terada-Old model	0.62	0.900	6.6	0.18	0.41	0.64
New-Old model	0.36	1.098	10.5	0.24	0.33	0.57
Terada-New model	0.64	0.805	5.6	0.24	0.52	0.62
New-New model	0.41	1.06	9.3	0.23	0.41	0.68
^{131}I air concentration from 15 March to 1 April 2011						
Terada-Old model	0.19	0.571	4.5	0.09	0.32	0.59
New-Old model	0.17	0.966	9.0	0.19	0.43	0.67
Terada-New model	0.12	-0.370	4.2	0.24	0.48	0.71
New-New model	0.25	0.211	3.9	0.26	0.37	0.59

Table S2. The calculated percentages of each deposition process to the total amount of ^{137}Cs released from 5:00 on 11 March to 0:00 on 1 April 2011 over the land (forest and other landuse categories) and sea in East Japan region (Domain 2; Fig. 3c).

	Deposition (%)					Outflow from the domain (%)
	Forest	Other land	All land	Sea	Land + Sea	
Wet deposition	14.2	5.5	19.7	6.6	26.3	–
Dry deposition	3.1	1.4	4.5	0.5	4.9	–
Fogwater deposition	0.8	0.7	1.5	0.2	1.7	–
Total deposition	18.0	7.7	27.7	7.3	33.0	67.0

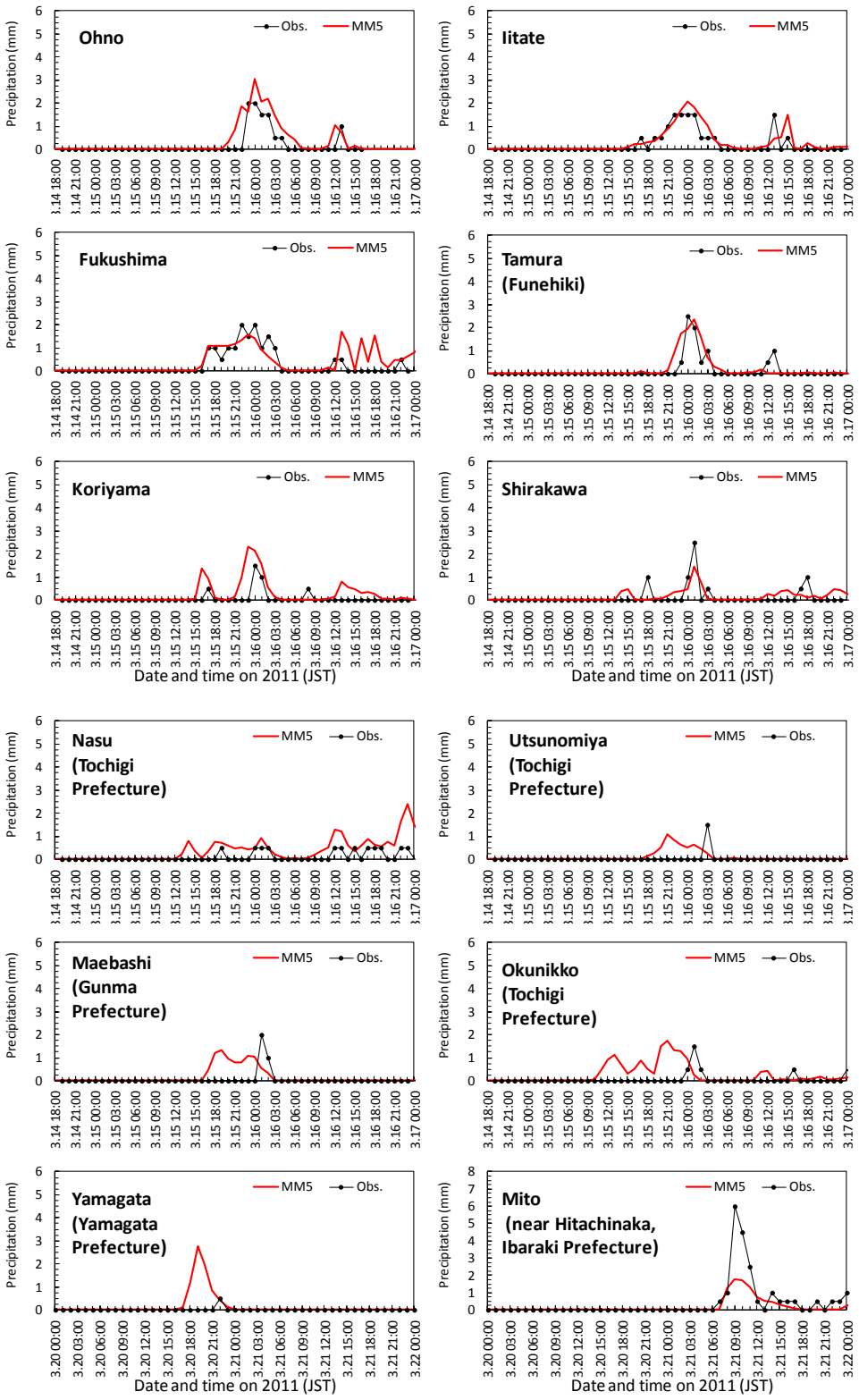

Figure S1. Temporal changes in calculated and observed hourly precipitation amount in East Japan on March 2011 in the WSPEEDI simulation. Locations of the comparisons were selected in several prefectures for those sites with high dose rates (Figs. 2 and 3c).

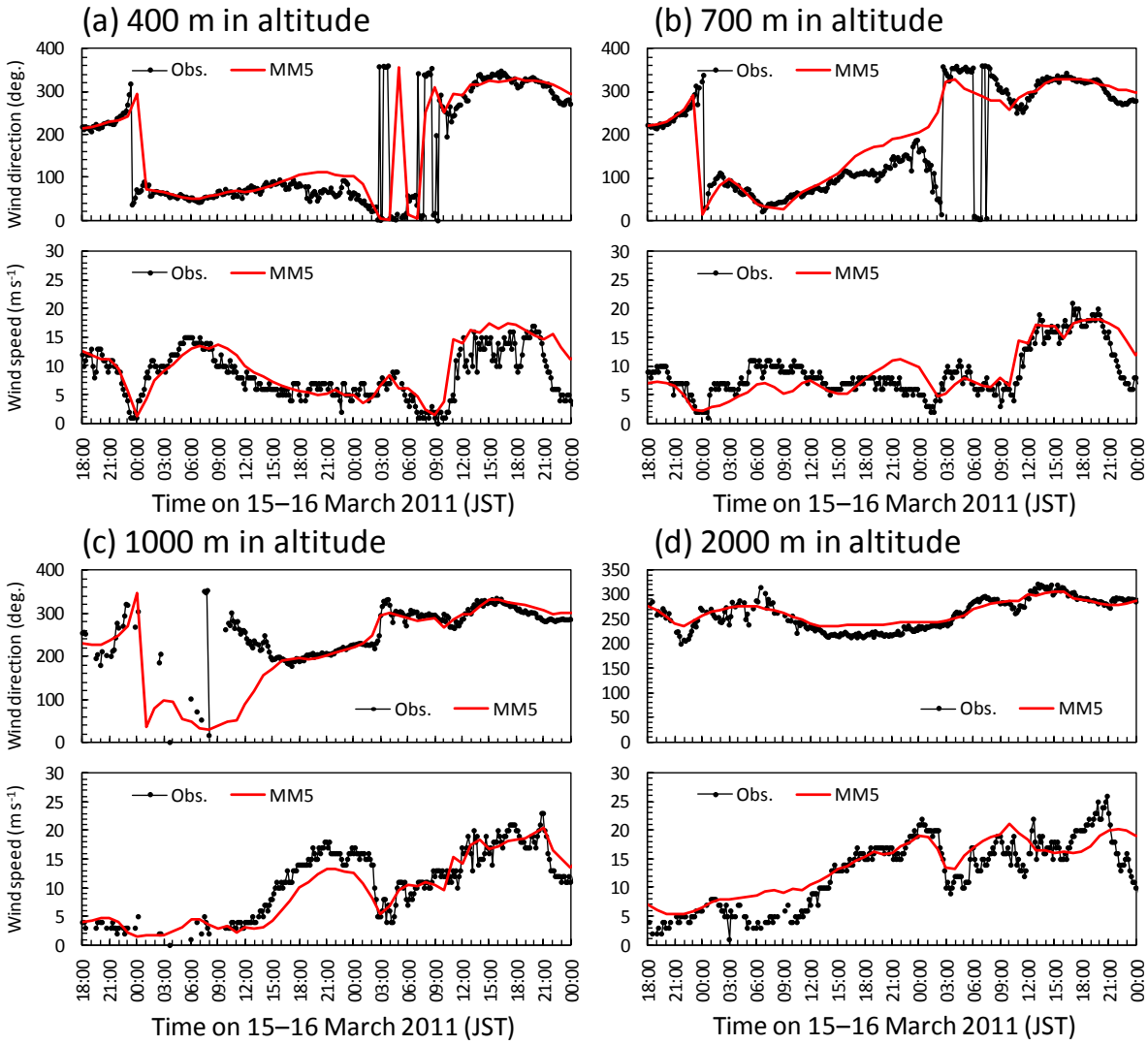

Figure S2. Temporal changes in the calculated and observed upper-air observations of wind and air temperature at (a) 400 m, (b)700 m, (c) 1000 m, and (d) 2000 m in altitude at Mito in Ibaraki Prefecture from 15–16 March 2011. The observational location is near the Japan Atomic Energy Agency (JAEA-Tokai) in Fig. 3c.

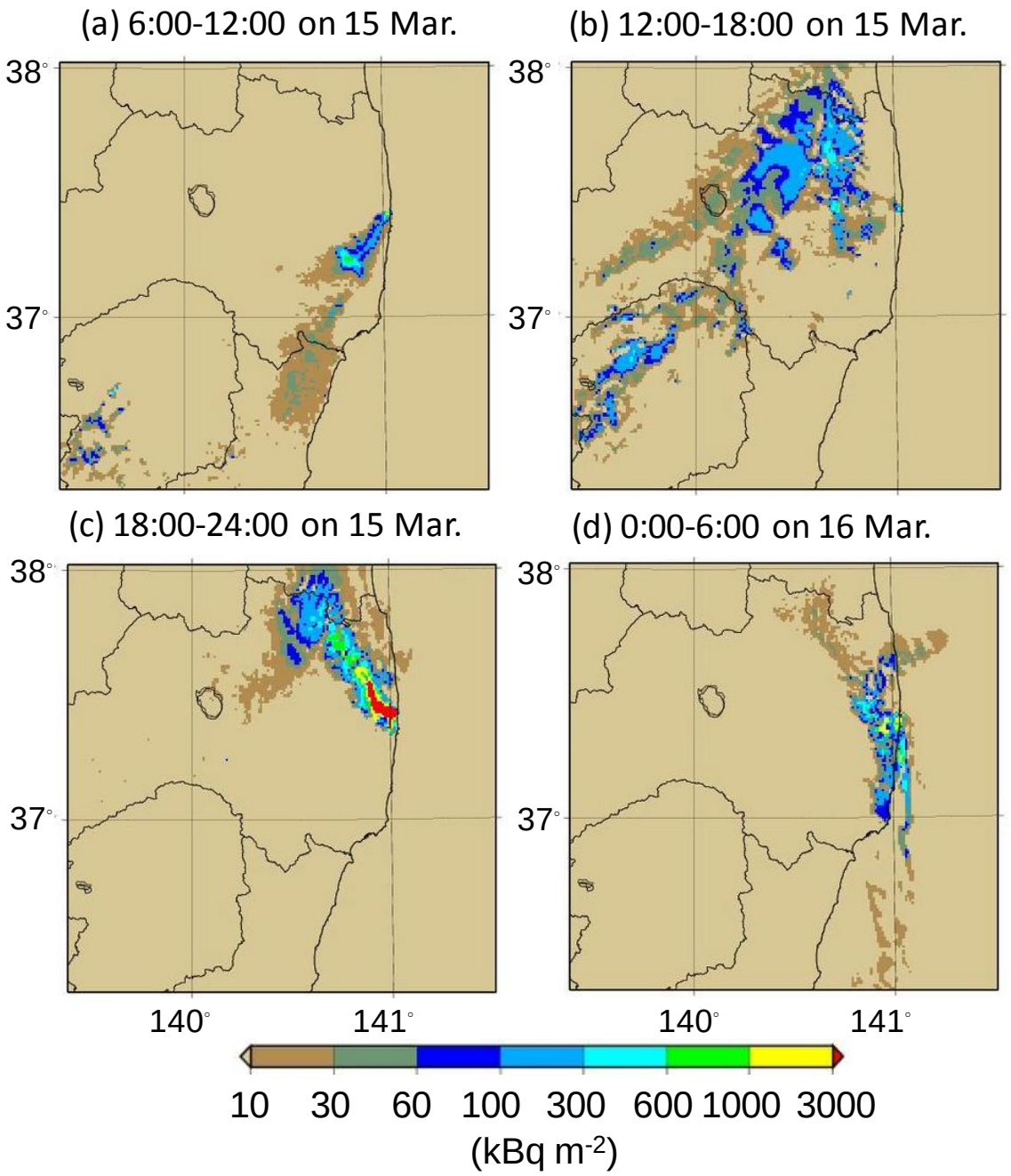

Figure S3. Spatial distributions of surface deposition of ^{137}Cs over East Japan accumulated during the periods of (a) 6:00–12:00 on 15 March, (b) 12:00–18:00 on 15 March, (c) 18:00–24:00 on 15 March, and (d) 0:00–6:00 on 16 March calculated by WSPEEDI-II using the new source term.

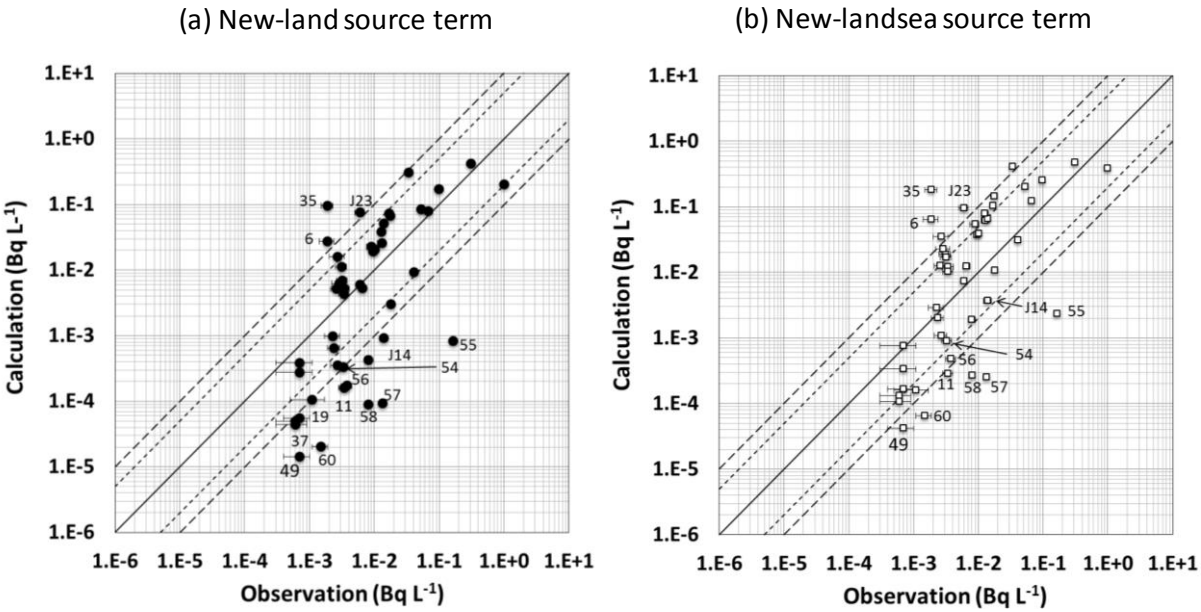

Figure S4. Scatter diagrams of ^{134}Cs sea surface concentration over the Pacific Ocean for measured and calculated values using (a) the source term land data only (referred as "New-land") and (b) both land and sea data (referred as "New-landsea").

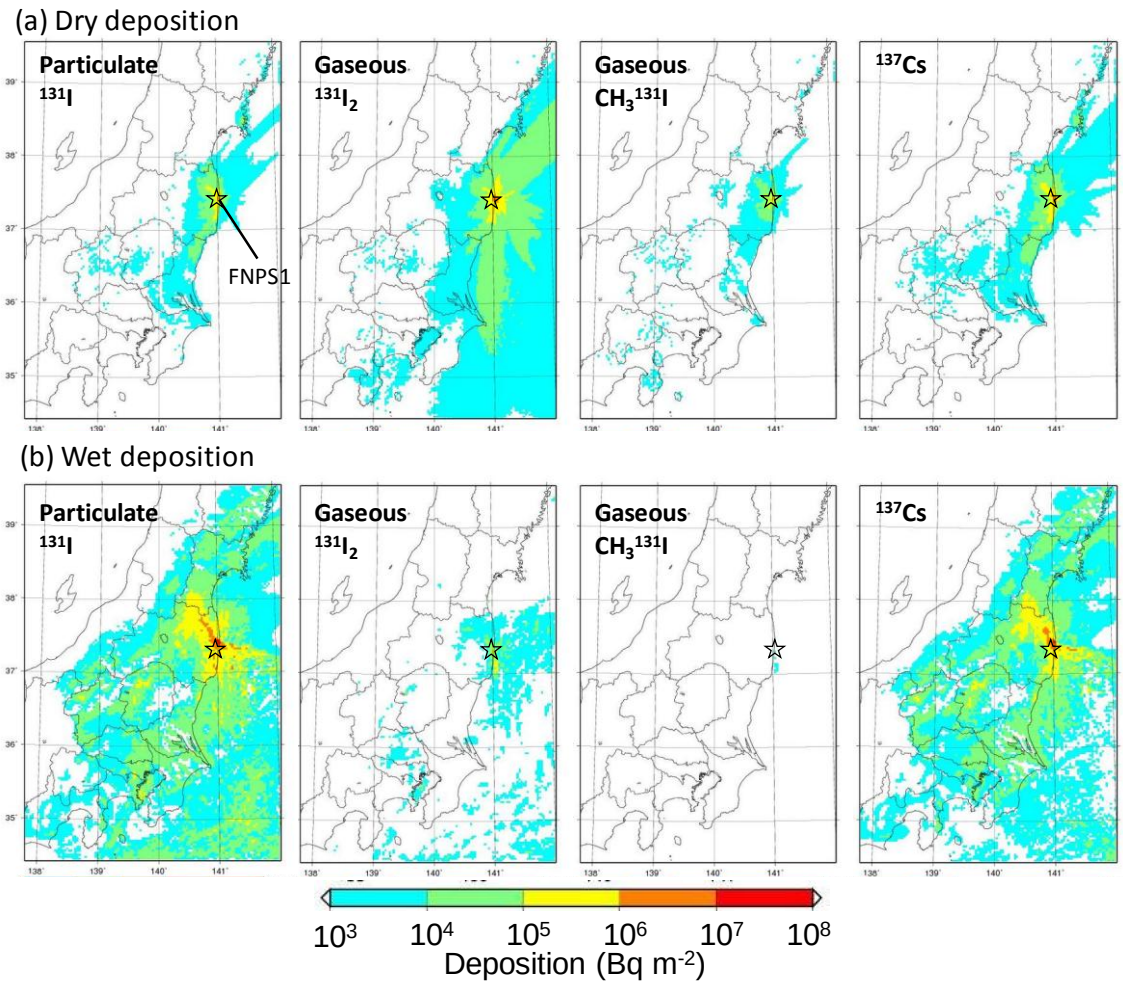

Figure S5. (a) Spatial distributions of the cumulative dry deposition and (b) wet deposition of each radionuclide (particulate and gaseous ^{131}I and ^{137}Cs) (Bq m^{-2}) at 0:00 on 1 April 2011 in the WSPEEDI simulation.

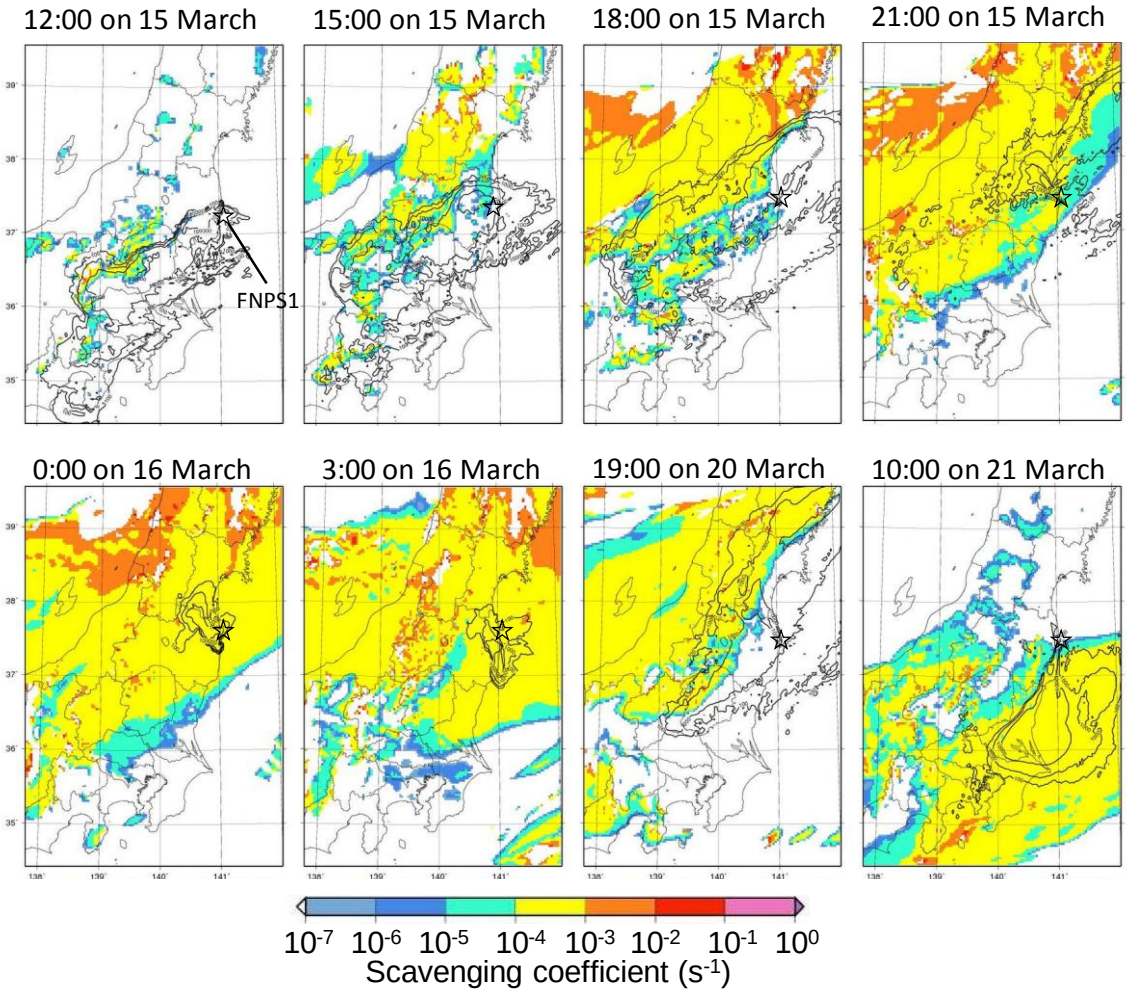

Figure S6. Spatial distributions of the scavenging coefficient, Λ (s^{-1}) calculated and observed meteorological variables in East Japan for 15–16, 20, and 21 March 2011 in the WSPEEDI simulation. Λ represents the vertical mean values for the atmospheric layers where the calculated ^{137}Cs concentration was greater than zero. The contour lines represent vertically accumulated concentration of ^{137}Cs.

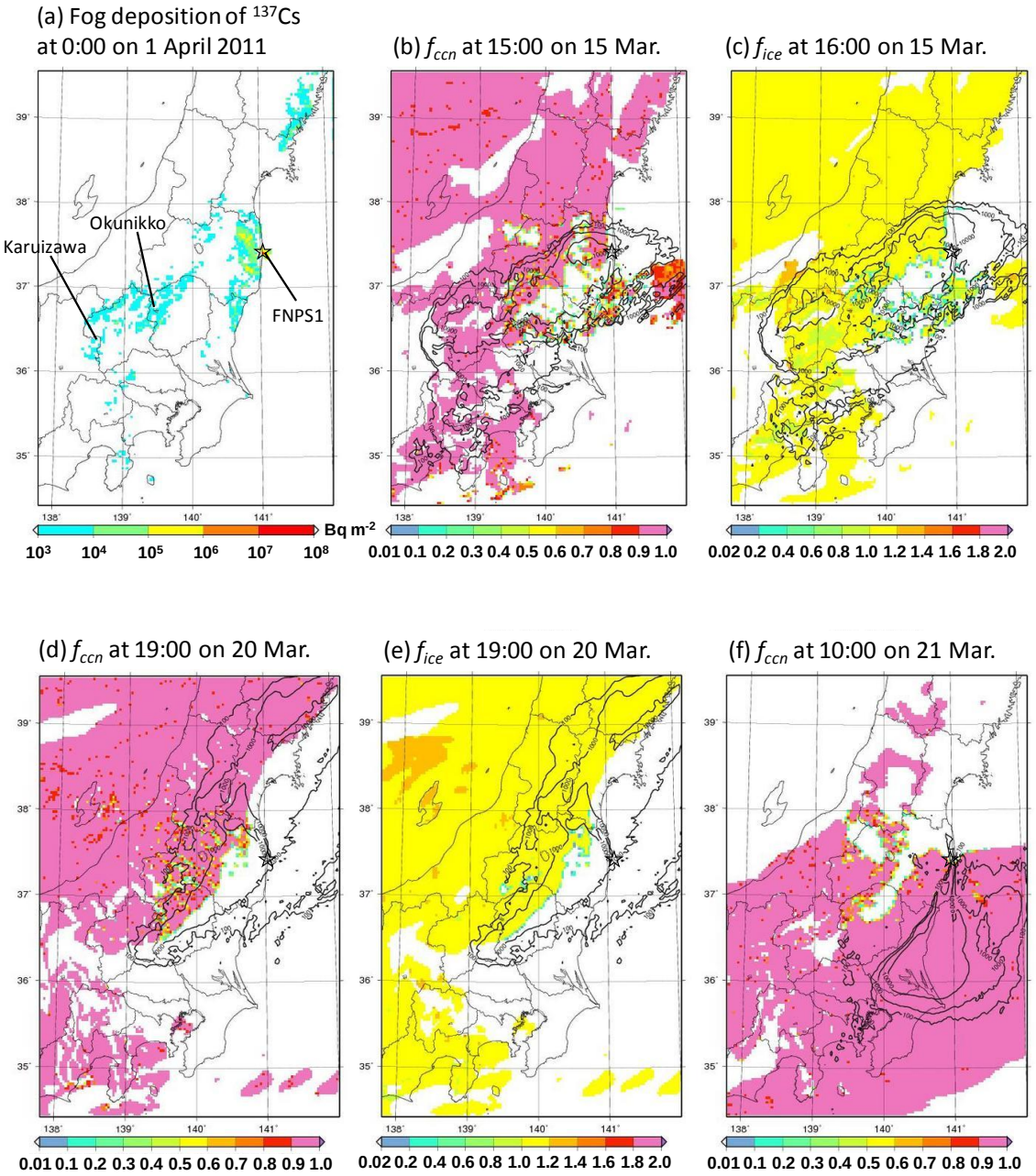

Figure S7. (a) Spatial distributions of cumulative fog deposition of ^{137}Cs (Bq m^{-2}) at 0:00 on 1 April 2011, and [(b), (d), (f)] the fraction of the CCN activated aerosols in cloud (f_{ccn}) (b) at 15:00 on 15 March, (d) 19:00 on 20 March, and (f) 10:00 on 21 March, and [(c), (e)] the accretion efficiency of cloud droplets by settling ice crystals (i.e., snow and graupel) (f_{ice}) (c) at 16:00 on 15 March and 19:00 on 20 March in the WSPEEDI simulation. f_{ccn} and f_{ccn} represent vertical mean values for the atmospheric layers where the calculated ^{137}Cs concentration was greater than zero. The contour lines in [(b)–(f)] represent vertically accumulated concentration of ^{137}Cs.

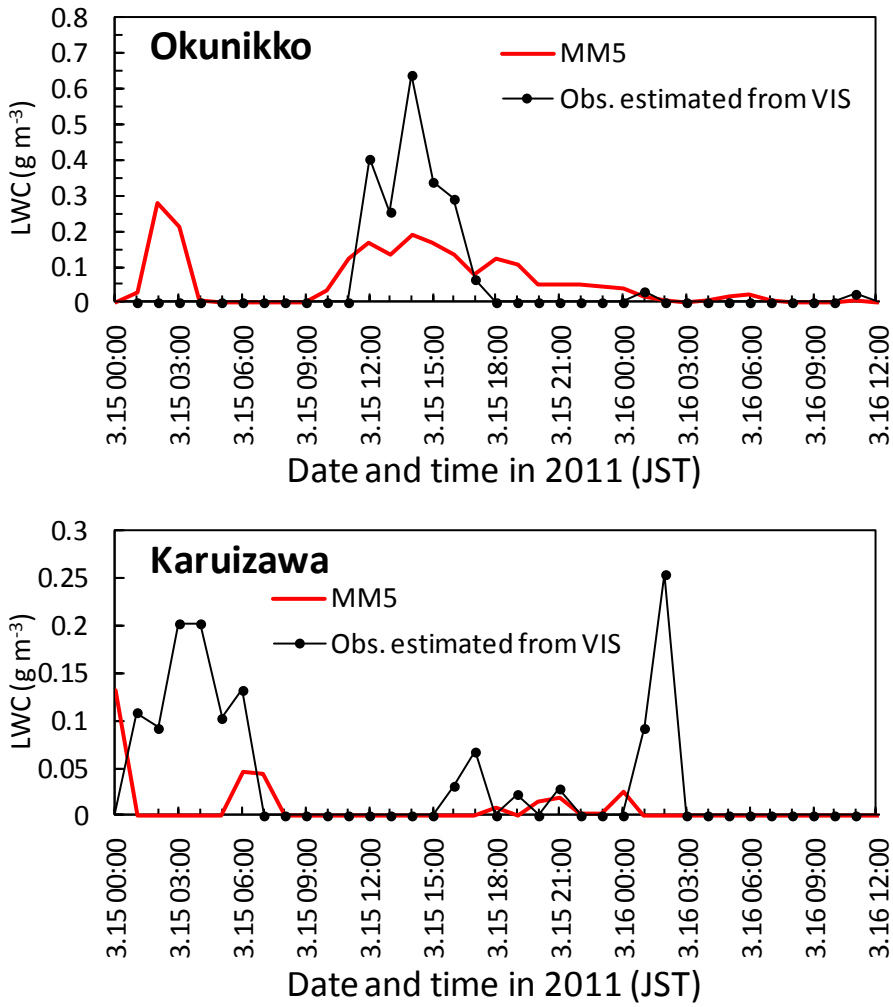

Figure S8. Temporal changes in the calculated and observed cloud liquid water content (CLW) near the surface at the meteorological surface station of Okunikko and Karuizawa in 15–16 March 2011. Locations of both stations are depicted in Fig. S7a. The observed CLW was derived from visibility (VIS) data using the empirical relationship between CLW and VIS proposed by Stoelinga and Warner (1999).

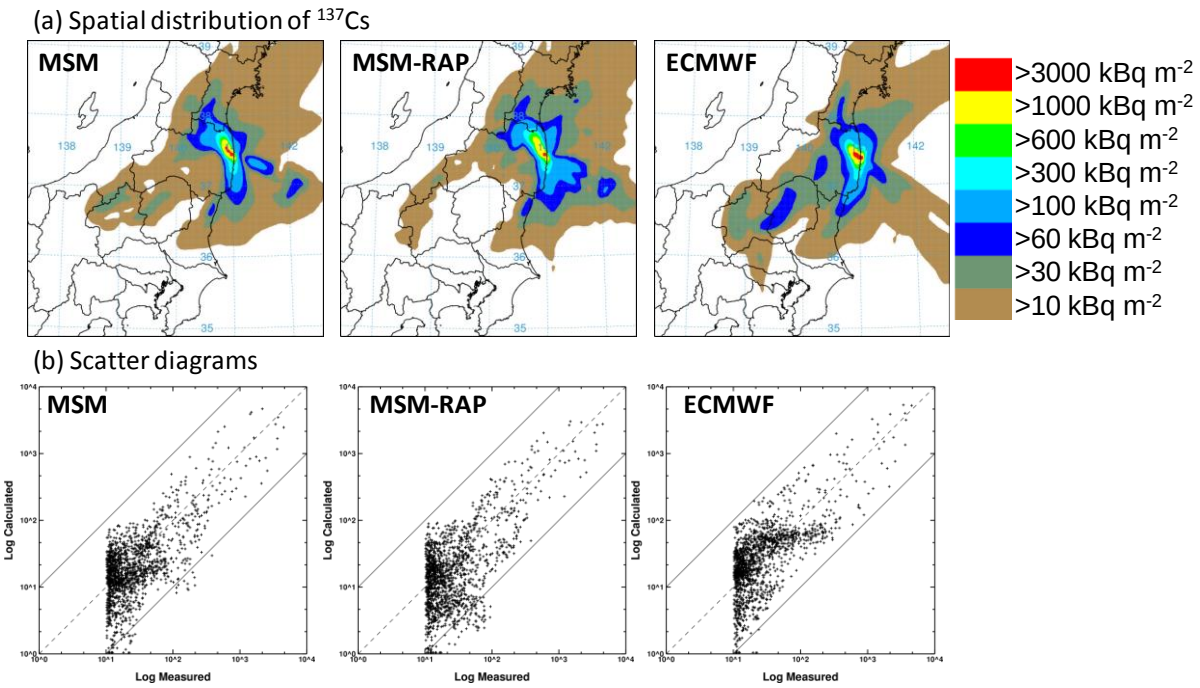

Figure S9. (a) Spatial distributions and (b) scatter diagrams of surface depositions of ^{137}Cs (kBq m^{-2}) on 1 April 2011 comparing measurements and calculations of NAME using the new source term using the three meteorological fields (MSM, MSM-RAP, and ECMWF).

References

Stoelinga, M.T., and Warner, T.T.: Nonhydrostatic, mesobeta-scale model simulations of cloud ceiling and visibility for an east coast winter precipitation event. J. Appl. Meteorol., 38, 385-404, 1999.